Check for updates

View Article Online
View Journal

Analyst

Accepted Manuscript

This article can be cited before page numbers have been issued, to do this please use: K. Takahashi, Y. Takeda, K. Nishiyama, M. Fukuyama, M. Maeki, A. Ishida, H. Tani, A. Imai, K. Shigemura, A. Hibara, H. Ogawa and M. Tokeshi, *Analyst*, 2026, DOI: 10.1039/D6AN00505E.

This is an Accepted Manuscript, which has been through the Royal Society of Chemistry peer review process and has been accepted for publication.

Accepted Manuscripts are published online shortly after acceptance, before technical editing, formatting and proof reading. Using this free service, authors can make their results available to the community, in citable form, before we publish the edited article. We will replace this Accepted Manuscript with the edited and formatted Advance Article as soon as it is available.

You can find more information about Accepted Manuscripts in the Information for Authors.

Please note that technical editing may introduce minor changes to the text and/or graphics, which may alter content. The journal's standard Terms & Conditions and the Ethical guidelines still apply. In no event shall the Royal Society of Chemistry be held responsible for any errors or omissions in this Accepted Manuscript or any consequences arising from the use of any information it contains.

View Article Online
DOI: 10.1039/D6AN00505E

Detection of H5 Subtype Avian Influenza Virus in Avian Oropharyngeal Swab Samples Using a Microfluidic Non-Competitive Fluorescence Polarization Immunoassay

Kazuki Takahashi[1], Yohei Takeda[2], Keine Nishiyama[1], Mao Fukuyama[3], Masatoshi Maeki[4], Akihiko Ishida[4], Hirofumi Tani[4], Ayuko Imai[5], Koji Shigemura[5], Akihide Hibara[6], Haruko Ogawa[7], Manabu Tokeshi[4,8,9]*

[1]*Graduate School of Chemical Sciences and Engineering, Hokkaido University, Kita 13 Nishi 8, Kita-ku, Sapporo 060-8628, Japan*
[2]*Department of Veterinary Medicine, Obihiro University of Agriculture and V*eterinary *Medicine, 2-11 Inada, Obihiro, Hokkaido 080-8555, Japan*
[3]*Institute of Multidisciplinary Research for Advanced Materials, Tohoku University, 2-1-1, Katahira, Aoba-ku, Sendai 980-8577, Japan*
[4]*Division of Applied Chemistry, Faculty of Engineering, Hokkaido University, Kita 13 Nishi 8, Kita-ku, Sapporo 060-8628, Japan*
[5]*Tianma Japan, Ltd., Shinkawasaki Twin Tower West 28F, 1-1-2, Kashimada, Saiwai-ku, Kawasaki 212-0058, Japan*
[6]*Department of Chemistry, School of Science, Institute of Science Tokyo, 2-12-1 Ookayama, Meguro-ku, Tokyo 152-8551, Japan*
[7]*Research Center for Global Agromedicine, Obihiro University of Agriculture and Veterinary Medicine, 2-11 Inada, Obihiro, Hokkaido 080-8555, Japan*
[8]*Inovative Research Center for Preventive Medical Engineering, Nagoya University, Furo-cho, Chikusa-ku, Nagoya 464-8603, Japan*
[9]*Institute of Nano-Life Systems, Institutes of Innovation for Future Society, Nagoya University, Furo-Cho, Chikusa-ku, Nagoya 464-8603, Japan*

*Corresponding author.

E-mail address: tokeshi@eng.hokudai.ac.jp (M.T).

Open Access Article. Published on 11 June 2026. Downloaded on 6/12/2026 3:26:18 AM.
This article is licensed under a Creative Commons Attribution 3.0 Unported Licence.

Analyst Accepted Manuscript

View Article Online
DOI: 10.1039/D6AN00505E

Abstract

Rapid and simple methods for on-site detection of avian influenza virus (AIV) are essential for effective field surveillance. In this study, a microfluidic device-based non-competitive fluorescence polarization immunoassay (NC-FPIA) using an ATTO 647N-labeled hemagglutinin fragment of H5-AIV as a tracer was developed for the quantification of H5 subtype AIV (H5-AIV) in avian oropharyngeal swab samples. Autofluorescence from the swab matrix significantly interfered with fluorescence polarization measurements. However, quantitative detection of H5-AIV was achieved by suppressing the matrix effect through 80-fold dilution. The limit of detection was 186.4 μg/mL. The assay can be completed within 20 minutes without complex sample preparation, making it suitable for rapid on-site applications, including field surveillance of AIV in wild birds and poultry. Furthermore, by designing appropriate tracers, the method can be extended to other AIV subtypes.

Open Access Article. Published on 11 June 2026. Downloaded on 6/12/2026 3:26:18 AM.
This article is licensed under a Creative Commons Attribution 3.0 Unported Licence.

Analyst Accepted Manuscript

View Article Online
DOI: 10.1039/D6AN00505E

Open Access Article. Published on 11 June 2026. Downloaded on 6/12/2026 3:26:18 AM.
This article is licensed under a Creative Commons Attribution 3.0 Unported Licence.

Introduction

In 2024, highly pathogenic avian influenza virus (HPAIV) was detected in dairy cattle in the United States for the first time[1,2], and human infections among dairy farm workers were also reported[3]. Such cross-species transmission has raised public health concerns, as it may indicate the potential for future adaptation of the virus to humans. In addition, HPAIV is transmitted from wild birds to poultry worldwide, leading to outbreaks that result in large-scale culling and supply disruptions. Consequently, significant economic impacts have been observed, including increases and volatility in the prices of poultry products such as chicken meat and eggs[4]. Thus, HPAIV poses a serious threat not only to public health but also to economic and social activities, highlighting the need to strengthen global surveillance systems from a One Health perspective[5,6]. Among HPAIV subtypes, the H5N1 influenza virus is under intensive global surveillance as one of the most likely candidates for the next pandemic, owing to its documented human infections and high severity[7]. In addition, the H7N9 influenza virus[8] and H5N6 influenza virus[9], which have been reported to infect humans and are associated with severe disease, are also important targets of surveillance, along with subtypes such as the H5N8 influenza virus[10], H9N2 influenza virus[11], and H5N3 influenza virus[12], which are considered to pose potential risks.

Current surveillance of avian influenza virus (AIV) relies on rapid antigen tests such as lateral flow assays (LFAs)[13,14] for on-site screening, enzyme-linked immunosorbent assays (ELISAs)[14] for laboratory-based antigen and antibody detection, and RT-PCR[14,15] for confirmatory diagnosis. However, LFAs are generally limited to qualitative or semi-qualitative analysis and often suffer from insufficient sensitivity, particularly in complex biological specimens such as swab samples, serum, or tissue

Analyst Accepted Manuscript

View Article Online
DOI: 10.1039/D6AN00505E

Open Access Article. Published on 11 June 2026. Downloaded on 6/12/2026 3:26:18 AM.
This article is licensed under a Creative Commons Attribution 3.0 Unported Licence.

extracts, whereas ELISAs and RT-PCR typically require longer processing times and specialized laboratory facilities, making them less suitable for field deployment. These limitations highlight the need for diagnostic platforms that combine high sensitivity with field deployability[16]. In particular, for field surveillance of wild birds and poultry, analytical systems capable of rapidly processing small-volume samples with minimal pretreatment are highly desirable.

We previously developed a portable fluorescence polarization analyzer incorporating a disposable microfluidic device suitable for on-site analysis[17,18]. To date, by combining this analyzer with fluorescence polarization immunoassay (FPIA), we have successfully achieved simple and rapid analysis of mycotoxins[19] and marine toxins[20,21] using competitive assays, as well as proteins[22], antibodies[23,24], exosomes[25], and viruses[26,27] using non-competitive assays. Conventional FPIA is a homogeneous immunoassay based on a competitive assay in which a fluorescently labeled analyte (tracer) and the unlabeled analyte (target) compete for binding to a specific antibody[28]. In contrast, non-competitive FPIA (NC-FPIA) is also a homogeneous immunoassay based on a non-competitive assay, in which fluorescently labeled antibody fragments[29], protein fragments[23,24], nanobodies[22], peptides[25], or aptamers[27] that specifically recognize the target analyte are used as tracers to bind to the analyte.

Specifically, our developed method for the detection of anti-H5 AIV antibodies[23] and H5 subtype AIV (H5-AIV)[26], was combined with a fluorescence polarization analyzer using NC-FPIA for application to the field surveillance of wild birds and poultry. For antibody detection, we successfully achieved the selective detection of anti-H5 AIV antibodies from antisera containing H1-H16 subtypes using a fluorescently labeled hemagglutinin (HA) fragment of H5-AIV as a tracer. The method required only 2 μL of

Analyst Accepted Manuscript

View Article Online
DOI: 10.1039/D6AN00505E

Open Access Article. Published on 11 June 2026. Downloaded on 6/12/2026 3:26:18 AM.
This article is licensed under a Creative Commons Attribution 3.0 Unported Licence.

serum and a 20 min analysis time, demonstrating rapid analysis with a minimal sample volume and therefore, it is well suited for fast on-site surveillance. For virus detection, we demonstrated preliminary detection of H5-AIV using a fluorescein-labeled antibody fragment (Fab) that recognizes the HA of H5-AIV as a tracer. This result represents, to the best of our knowledge, the first reported example of detecting virus particles using FPIA. However, the samples were prepared in phosphate-buffered saline (PBS), and we anticipated that detection in real samples, such as avian swabs and serum, would be more challenging in terms of sensitivity.

Therefore, in this study, we aimed to develop a practical NC-FPIA-based method for the detection of H5-AIV suitable for on-site analysis. Because FPIA is based on fluorescence detection, it is affected by sample autofluorescence. We measured the autofluorescence of avian oropharyngeal swab samples and viral transport medium (VTM) and selected fluorophores with low susceptibility to autofluorescence interference. Since fluorescence polarization (P) is also influenced by the fluorescence lifetime of the fluorophore[30], we prepared tracers labeled with two different fluorophores having distinct fluorescence lifetimes and evaluated their performance. Based on these results, we optimized the tracer and successfully quantified H5-AIV in avian oropharyngeal swab samples. These results suggest that the present method has potential for use in on-site surveillance of H5-AIV in wild birds and poultry and may be extended to other subtype AIVs through appropriate tracer design. The present study provides a practical framework for applying FPIAs to real-world biological samples.

Experimental

Materials and chemicals

Analyst Accepted Manuscript

View Article Online
DOI: 10.1039/D6AN00505E

Open Access Article. Published on 11 June 2026. Downloaded on 6/12/2026 3:26:18 AM.
This article is licensed under a Creative Commons Attribution 3.0 Unported Licence.

Anti-H5 HA polyclonal antibody (anti-H5-HA rabbit IgG polyclonal antibody) was purchased from Bioss Antibodies (MA, USA). Bovine serum albumin (BSA) was purchased from Fujifilm Wako Pure Chemical Corporation (Osaka, Japan). HiLyte Fluor™ 647 Labeling Kit-NH_2 and ATTO 647N NHS ester were purchased from Dojindo Laboratories, Inc. (Kumamoto, Japan) and AAT Bioquest, Inc. (CA, USA), respectively. VTM was procured from Elmex Co., Ltd. (Tokyo, Japan). The Micro BCA Protein Assay Kit and PBS were purchased from Thermo Fisher Scientific, Inc. (MA, USA).

Preparation of inactivated H5N3 AIV

Two H5N3 subtype AIV strain, A/whistling/swan/Shimane/499/1983 (Shimane strain) and A/duck/Hong Kong/820/80 (Hong Kong strain) were kindly provided by Dr. Toshihiro Ito (Tottori University, Japan) and Dr. Yoshihiro Sakoda (Hokkaido University, Japan), respectively. These H5N3 AIVs were propagated in the allantoic cavities of 10- to 11-day-old embryonated chicken eggs for 3- to 4-days. The harvested allantoic fluid (AF) was subjected to ultracentrifugation (25,000 rpm, 2h; Optima L-70K Ultracentrifuge, Beckman Coulter, Inc., CA, USA), and the viral pellet was resuspended in PBS to obtain a 500- to 1000-fold concentrated virus suspension. The virus was further purified by ultracentrifugation (43000 rpm, 2h; Himac CS-GXII 100 GXL, Hitachi Koki Co., Ltd., Tokyo, Japan) with 30% and 60% (w/v) sucrose solutions. The viral band at the 30%/60% interface was collected, diluted with PBS, and centrifuged again (43,000 rpm, 2 h) to remove sucrose. The final pellet was resuspended in PBS. Protein concentration was determined using a Micro BCA protein assay and adjusted to 1 mg/mL with PBS. For inactivation, 10% buffered formalin was added to a final concentration of 0.1%, and the suspension was incubated at 37°C for 40 h. Residual formalin was neutralized with

Analyst Accepted Manuscript

View Article Online
DOI: 10.1039/D6AN00505E

sodium hydrosulfite (final concentration ~0.6%), followed by dialysis twice against 1000 volumes of PBS using regenerated cellulose membranes (MWCO 8,000; Repligen Corporation, MA, USA) to remove residual reagents. After dialysis, the concentration of inactivated H5N3 AIVs was measured again and adjusted to 0.5 mg/mL with PBS.

Preparation of tracers

Two types of tracers were synthesized by Hokudo Co., Ltd. (Sapporo, Japan) according to the following procedure. The anti-H5-HA rabbit IgG polyclonal antibodies were fragmented by papain digestion and purified using Protein A. The amino groups of the Fab fragments were labeled with HiLyte Fluor™ 647 and ATTO 647N according to the respective manufacturers' instructions. Unreacted fluorescent dyes were removed using a modified polyethersulfone membrane (Nanosep 3K Omega, Pall Corporation, NY, USA). The concentrations of the Fab fragments and fluorescent dyes were determined based on the absorbance at 280 nm and 500 nm measured using a fluorometer (NanoDrop One, Thermo Fisher Scientific, Inc.). The labeling efficiency (dye concentration/Fab fragment concentration) was 6.65 for HiLyte Fluor™ 647 and 5.22 for ATTO 647N.

Fluorescence and microfluidic-based fluorescence polarization measurement

To evaluate background fluorescence in fluorescence polarization measurements under conditions relevant to real-sample analysis, three-dimensional fluorescence spectra of oropharyngeal swab samples and VTM were measured. After tenfold dilution with ultrapure water, each sample was introduced into a quartz cuvette and analyzed by three-dimensional fluorescence (excitation-emission matrix, EEM) spectroscopy using a spectrofluorometer (F-7000, Hitachi High-Tech Corporation, Ibaraki, Japan) with

Open Access Article. Published on 11 June 2026. Downloaded on 6/12/2026 3:26:18 AM.
This article is licensed under a Creative Commons Attribution 3.0 Unported Licence.

Analyst Accepted Manuscript

View Article Online
DOI: 10.1039/D6AN00505E

Open Access Article. Published on 11 June 2026. Downloaded on 6/12/2026 3:26:18 AM.
This article is licensed under a Creative Commons Attribution 3.0 Unported Licence.

excitation and emission wavelength ranges of 300- to 650 nm and 300- to 700 nm, respectively.

Fluorescence polarization measurements were carried out using a portable multichannel fluorescence polarization analyzer equipped with microfluidic devices (Fig. 1), as described previously[17,18,23]. In this study, the excitation and emission wavelengths were modified. The analyzer was operated with an excitation wavelength of 625 nm, and fluorescence emission was collected through an emission filter covering the wavelength range of 663- to 734 nm.

Binding activity assay of two tracers with H5N3 AIV

To determine the optimal tracer concentration, the binding activities of the two synthesized tracers, HiLyte Fluor™ 647-labeled Fab fragment (HiLyte-Fab) and ATTO 647N-labeled Fab fragment (ATTO-Fab), with purified H5N3 AIV were evaluated. Stock solutions of HiLyte-Fab (0.158 mg/mL) and ATTO-Fab (0.58 mg/mL) were diluted with PBS to prepare tracer solutions at concentrations of 60, 120, 240, and 480 ng/mL, respectively. A 1% BSA solution was prepared by dissolving BSA in PBS. Purified H5N3 AIV in PBS, HiLyte-Fab or ATTO-Fab solution, 1% BSA solution, and PBS were added to a 0.5 mL microtube. The mixing ratio of H5N3 AIV, fluorescently labeled Fab, 1% BSA solution, and PBS was 2:1:1:6 (total volume, 50 µL). The mixture was incubated at 25 °C for 15 min. Subsequently, an aliquot of the mixture (12 µL) was introduced into the microfluidic device. The microfluidic device was then set in the portable multichannel fluorescence polarization analyzer, and the fluorescence polarization (P) was measured in triplicate for each concentration.

Analyst Accepted Manuscript

View Article Online
DOI: 10.1039/D6AN00505E

Open Access Article. Published on 11 June 2026. Downloaded on 6/12/2026 3:26:18 AM.
This article is licensed under a Creative Commons Attribution 3.0 Unported Licence.

Quantification of H5N3 AIV using NC-FPIA

Purified H5N3 AIV was serially diluted twofold with PBS to prepare seven samples covering a concentration range of 6.6-850 μg/mL. Each diluted H5N3 AIV sample was mixed with ATTO-Fab at a fixed concentration of 120 ng/mL, 1% BSA solution, and PBS in a 0.5 mL microtube at a volume ratio of 7:1:1:1, resulting in a total sample volume of 50 μL. The mixture was incubated at 25 °C for 15 min. For blank measurements, PBS, ATTO-Fab, and 1% BSA solution were mixed at a ratio of 8:1:1 (50 μL). Fluorescence polarization measurements were performed in triplicate for each sample using the portable multichannel fluorescence polarization analyzer under the conditions described above.

Quantification of H5N3 AIV in avian oropharyngeal swab using NC-FPIA

Oropharyngeal swabs were collected from wild birds captured in Hokkaido and individual immersed in 1 mL of VTM. Swab samples obtained from approximately 20 individuals confirmed to be negative for influenza A virus were used as avian oropharyngeal swab samples in this study. To evaluate the autofluorescence of avian oropharyngeal swab samples, swab samples diluted 10- to 160-fold in PBS and ATTO-Fab (120 ng/mL) in PBS were each added (120 μL) to a 96-well black microplate (ProteoSave^{TM} 96F Plate (Black), Sumitomo Bakelite Co., Ltd., Tokyo, Japan), and the fluorescence intensity was measured using a plate reader (Infinite 200 PRO F Plex, Tecan, Männedorf, Switzerland) at an excitation wavelength of 620 nm and an emission wavelength of 670 nm. In the detection of H5N3 AIV in avian oropharyngeal swab samples, purified H5N3 AIV, diluted swab samples, 120 ng/mL ATTO-Fab, and 1% BSA solution were mixed in a 0.5 mL microtube at a volume ratio of 7:1:1:1 (50 μL) and

Analyst Accepted Manuscript

View Article Online
DOI: 10.1039/D6AN00505E

incubated at 25 °C for 15 min. Fluorescence polarization measurements were performed in triplicate for each sample using the portable multichannel fluorescence polarization analyzer under the conditions described above.

Results and discussion

Selection of a tracer

In general, when measuring real samples, signals originating from interfering substances other than the target analyte contribute to the background. Therefore, the EEM spectra of an avian oropharyngeal swab sample and VTM were measured (Fig. S1†). VTM was not only present in the swab samples used in this study, but it is also widely used as a medium for preserving and transporting samples collected from wild birds and poultry in the field, making it relevant to field surveillance. In previous studies, a fluorescein-labeled Fab that recognizes the HA of H5-AIV was used as a tracer[26]. Accordingly, the portable fluorescence polarization analyzer was configured with an excitation wavelength of 470 nm and an emission detection range of 515- to 525 nm. Under these conditions, fluorescence was observed in both EEM spectra, indicating potential background interference. Notably, the swab sample exhibited stronger fluorescence than VTM. Based on these results, two fluorescent dyes, HiLyte Fluor™ 647 and ATTO 647N, were selected. These dyes have excitation wavelengths of approximately 644- to 649 nm and emission wavelengths of approximately 669- to 672 nm, where background interference is minimal.

Next, tracers labeled with these dyes were prepared, and their performance was evaluated. As in our previous work[26], these dyes were conjugated to Fab fragments that recognize the HA of H5-AIV, and HiLyte-Fab and ATTO-Fab were synthesized. Figure

Open Access Article. Published on 11 June 2026. Downloaded on 6/12/2026 3:26:18 AM.
This article is licensed under a Creative Commons Attribution 3.0 Unported Licence.

Analyst Accepted Manuscript

View Article Online
DOI: 10.1039/D6AN00505E

Open Access Article. Published on 11 June 2026. Downloaded on 6/12/2026 3:26:18 AM.
This article is licensed under a Creative Commons Attribution 3.0 Unported Licence.

2 shows a schematic illustration of NC-FPIA. Free fluorophore-labeled Fab undergoes rapid rotational motion in solution. Therefore, even when excited with polarized light, the polarization of the emitted fluorescence is lost and randomized. As a result, the polarization value, $P = (P_{\parallel} - P_{\perp})/(P_{\parallel} + P_{\perp})$, becomes low, where $P_{\parallel}$ and $P_{\perp}$ represent the fluorescence intensities measured parallel and perpendicular to the excitation polarization, respectively. In contrast, when the fluorophore-labeled Fab binds to the HA of H5-AIV, the rotational motion of the resulting complex becomes slower. Consequently, the emitted fluorescence maintains its polarization, and the P increases. To investigate the polarization properties of both tracers, P was measured as a function of tracer concentration using an H5N3 AIV standard solution (850 μg/mL) (Fig.3). The y-axis represents the polarization change (ΔP), defined as the difference in polarization between the solution containing H5N3 AIV and the control (without H5N3 AIV), expressed as ΔmP ($\Delta P \times 10^3$). This is because the tracer itself has an intrinsic polarization, and using the difference eliminates the influence of the control, making it easier to evaluate the changes induced by the immunoreaction. The ΔP reached a maximum over a tracer concentration range of 60- to 120 ng/mL for HyLite-Fab and at 120 ng/mL for ATTO-Fab, and decreased at higher concentrations for both. This is likely due to saturation of viral binding sites and an increase in unbound tracer, which reduces the bound fraction and thereby diminishes the observed ΔP. In a comparison of the two tracers, ATTO-Fab exhibited a larger ΔP than HiLyte-Fab. Based on these results, ATTO-Fab was selected as the tracer for H5-AIV detection. In all subsequent experiments, ATTO-Fab at 120 ng/mL was used as the tracer.

The selection of ATTO 647N and HiLyte Fluor 647 was based on their long-wavelength fluorescence with low background, as well as their different fluorescence

Analyst Accepted Manuscript

View Article Online
DOI: 10.1039/D6AN00505E

Open Access Article. Published on 11 June 2026. Downloaded on 6/12/2026 3:26:18 AM.
This article is licensed under a Creative Commons Attribution 3.0 Unported Licence.

lifetimes, since fluorescence polarization depends on the fluorescence lifetime of the dye. The larger ΔP observed for ATTO-Fab compared to HiLyte-Fab can be rationalized by the Perrin equation[31]:

$$P = P_0 / (1 + \tau/\theta)$$

where P is the fluorescence polarization, P_0 is the fundamental polarization, τ is the fluorescence lifetime, and θ is the rotational correlation time, which depends on the molecular size of the fluorophore-target complex. In the present study, the fluorescence lifetimes of ATTO 647N and HiLyte Fluor™ 647 are 3.5 ns[32] and 1.0 ns[33], respectively. The molecular weight of the Fab fragment is approximately 50 kDa, and the contribution of the fluorophore (843 Da[34] for ATTO 647N and 1303 Da[33] for HiLyte 647) is negligible. Therefore, the rotational correlation times of ATTO-Fab and HiLyte-Fab in the free (unbound) state can be considered nearly identical. Under these conditions, the longer fluorescence lifetime of ATTO-Fab results in a larger τ/θ value, leading to greater depolarization and thus a lower polarization compared to HiLyte-Fab. Consistent with this expectation, the polarization values of the free tracers were 180 mP for ATTO-Fab and 225 mP for HiLyte-Fab (data not shown). Upon binding to the avian influenza virus, which is a large particle with a diameter of approximately 80- to 120 nm[35] and an effective molecular weight on the order of 10^8 Da, as estimated from its size and composition, the rotational correlation time becomes extremely large ($\theta >> \tau$), and the polarization approaches the limiting value P_0 for both tracers. Consequently, the difference between the free and bound states ($\Delta P = P_{bound} - P_{free}$) is larger for ATTO-Fab than for HiLyte-Fab, primarily due to its lower initial polarization in the free state.

Quantification of H5N3 AIV using NC-FPIA

Analyst Accepted Manuscript

View Article Online
DOI: 10.1039/D6AN00505E

Open Access Article. Published on 11 June 2026. Downloaded on 6/12/2026 3:26:18 AM.
This article is licensed under a Creative Commons Attribution 3.0 Unported Licence.

Figure 3 shows the calibration curve for purified H5N3 AIV in PBS. The Δ*P* increased with increasing H5N3 AIV concentration, demonstrating that purified H5N3 AIV can be quantified using the developed ATTO-Fab-based NC-FPIA. The limit of detection (LOD) for H5N3 AIV was determined to be 96 μg/mL, based on the average blank signal (control) plus three standard deviations. Although a strict direct comparison is not possible due to differences in dye and instrument optical properties as well as tracer concentration, comparison with the previous study[26] suggests that the present results may be more suitable for real sample analysis. In general, NC-FPIA exhibits a lower LOD when a lower tracer concentration is used[29]. Therefore, in the previous study employing a lower tracer concentration of 80 ng/mL, the LOD was slightly better than that of the present work. However, in that study, Δ*P* appeared to be saturated in the high-concentration region of H5N3 AIV, with a maximum Δ*P* of only 13 mP, which may limit its applicability to real samples with high background signals. In contrast, in the present study, no saturation of Δ*P* was observed within the measured concentration range, and a larger signal change was obtained, with a maximum Δ*P* exceeding 30 m*P*.

Quantification of H5N3 AIV in avian oropharyngeal swab samples using NC-FPIA

Prior to quantifying H5N3 AIV in the avian oropharyngeal swab samples, the fluorescence intensity of the swab matrix itself was measured. Autofluorescence from the swab samples affects the measured *P* and should therefore be minimized as much as possible[36]. Figure 4 compares the fluorescence intensity of swab samples diluted 10- to 160-fold in PBS and that of a 120 ng/mL ATTO-Fab solution. The dotted line indicates the fluorescence intensity of the ATTO-Fab solution. The autofluorescence of the swab samples became lower than that of the ATTO-Fab solution upon 80-fold dilution. Under

Analyst Accepted Manuscript

View Article Online
DOI: 10.1039/D6AN00505E

this condition, although the effect of autofluorescence is not negligible, it is reduced to a level that allows fluorescence polarization measurements.

Figure 5 shows the calibration curve for H5N3 AIV in avian oropharyngeal swab samples. When 80-fold diluted swab samples were used, the ΔP values were slightly lower than those obtained in PBS, and the increased variability observed at low concentrations can be attributed to the reduced magnitude of the ΔP and the relatively stronger influence of matrix-derived background signals in swab samples. However, ΔP increased with increasing concentration of the virus, allowing its quantification by the ATTO-Fab-based NC-FPIA method. The LOD for H5N3 AIV was determined to be 186.4 μg/mL, calculated as the mean blank signal plus three standard deviations. This value is not sufficiently low, suggesting that further improvements are required to reliably detect field samples collected at different stages of infection. According to our estimation, while the current LOD would allow for the detection of high-titer samples during peak infection, it may lack sufficient sensitivity for low-titer samples. To address this limitation, we expect that further sensitivity enhancement can be achieved by utilizing fluorophores with longer fluorescence lifetimes or employing high-performance Fab fragments. Nevertheless, although the sensitivity is lower than that of PCR-based methods, the present approach enables rapid and simple analysis with minimal sample preparation, which is advantageous for on-site screening. This method enables analysis of swab samples within 20 minutes, making it suitable for rapid on-site applications, including field surveillance of AIV in wild birds and poultry, without complex sample preparation. In this study, H5N3 AIV was used as the target analyte. By preparing an appropriate tracer, the method can be extended not only to H5 AIV but also to other HA subtype viruses. These results demonstrate the feasibility of fluorescence polarization measurements in

Open Access Article. Published on 11 June 2026. Downloaded on 6/12/2026 3:26:18 AM.
This article is licensed under a Creative Commons Attribution 3.0 Unported Licence.

Analyst Accepted Manuscript

View Article Online
DOI: 10.1039/D6AN00505E

complex biological matrices. Although this study demonstrated the potential of NC-FPIA for on-site analysis of avian influenza viruses, validation using naturally infected samples was not included in the present study. As the next stage of this research, we plan to evaluate the applicability and performance of the proposed method using naturally infected samples and to compare its performance with gold-standard methods such as RT-PCR.

Conclusions

In this study, an ATTO-Fab-based NC-FPIA was developed for the quantification of H5-AIV in avian oropharyngeal swab samples. The effect of autofluorescence from the sample matrix was systematically evaluated, and appropriate dilution conditions were identified to enable fluorescence polarization measurements in complex biological samples. Although the sensitivity is lower than that of PCR-based methods, the present approach enables rapid analysis within 20 minutes with minimal sample preparation. These features make the method suitable for on-site screening and field surveillance of AIV in wild birds and poultry. On the other hand, while this study demonstrated the potential of NC-FPIA for on-site analysis of avian influenza virus, validation using naturally infected samples was not performed. Future studies will focus on improving the detection sensitivity, evaluating the applicability and performance of the proposed method using naturally infected samples, and comparing its performance with gold-standard methods such as RT-PCR.

In addition, the method can be extended to other HA subtype AIVs through appropriate tracer design, demonstrating its potential as a versatile platform for practical virus detection. In recent years, not only avian influenza but also livestock infectious

Open Access Article. Published on 11 June 2026. Downloaded on 6/12/2026 3:26:18 AM.
This article is licensed under a Creative Commons Attribution 3.0 Unported Licence.

Analyst Accepted Manuscript

View Article Online
DOI: 10.1039/D6AN00505E

diseases such as classical swine fever, as well as other zoonotic viral infections, have become global concerns. The present method is therefore expected to be applicable to on-site surveillance of these infectious diseases.

Author contributions

K. T., Y. T., K. N., H. O., and M. T. conceived and designed the study. K. T., Y. T., K. N., and M. T. contributed to data collection and analysis. K. T., K. N., M. F., M. M., A. I., H. T., A. I., K. S., A. H., and M. T. joined discussions and provided constructive suggestions. K. T., Y. T., and M. T. wrote the initial draft of the manuscript. Y. T., M. F., M. M., A. I., H. T., A. I., K. S., A. H., H. O., and M. T. critically reviewed and made improvements in the manuscript. All authors approved the final version of the manuscript.

Conflict of interest

There are no conflicts to declare.

Acknowledgements

This work was supported by the JST-SENTAN program JPMJSN16A2. M.T. gratefully acknowledges Ryoto Watanabe, a student in his laboratory, for his assistance in preparing the figures.

Open Access Article. Published on 11 June 2026. Downloaded on 6/12/2026 3:26:18 AM.
This article is licensed under a Creative Commons Attribution 3.0 Unported Licence.

Analyst Accepted Manuscript

View Article Online
DOI: 10.1039/D6AN00505E

Open Access Article. Published on 11 June 2026. Downloaded on 6/12/2026 3:26:18 AM.
This article is licensed under a Creative Commons Attribution 3.0 Unported Licence.

References

1. A. J. Eisfeld, A. Biswas, L. Guan, C. Gu, T. Maemura, S. Trifkovic, T. Wang, L. Babujee, R. Dahn, P. J. Halfmann, T. Barnhardt, G. Neumann, Y. Suzuki, A. Thompson, A. K. Swinford, K. M. Dimitrov, K. Poulsen, Y. Kawaoka, *Nature*, 2024, **633**, 426-432.
2. L. C. Caserta, E. A. Frye, S. L. Butt, M. Laverack, M. Nooruzzaman, L. M. Covaleda, A. C. Thompson, M. P. Koscielny, B. Cronk, A. Johnson, K. Kleinhenz, E. E. Edwards, G. Gomez, G. Hitchener, M. Martins, D. R. Kapczynski, D. L. Suarez, E. R. A. Morris, T. Hensley, J. S. Beeby, M. Lejeune, A. K. Swinford, F. Elvinger, K. M. Dimitrov, D. G. Diel, *Nature*, 2024, **634**, 669-676.
3. T. M. Uyeki, S. Milton, C. A. Hamid, C. R. Webb, S. M. Presley, V. Shetty, S. N. Rollo, D. L. Martinez, S. Rai, E. R. Gonzales, K. L. Kniss, Y. Jang, J. C. Frederick, J. A. De La Cruz, J. Liddell, H. Di, M. K. Kirby, J. R. Barnes, C. T. Davis, *N. Engl. J. Med.*, 2024, **390**, 2028-2029.
4. Z. Nisaa, B. Häsler, H. Bannani, R. Jorquera, F. Scolamacchia, P. Alarcon, *Prev. Vet. Med.*, 2026, **251**, 106827.
5. Food and Agriculture Organization of the United Nations. One Health approach to avian influenza: Protecting food security and human health. https://www.fao.org/one-health/highlights/one-health-approach-to-avian-influenza/en (accessed April 10, 2026).
6. European Commission. A One Health approach to zoonotic avian influenza. https://health.ec.europa.eu/one-health/zoonotic-threats/one-health-approach-zoonotic-avian-influenza_en (accessed April 10, 2026).
7. World Health Organization. Global Influenza Programme. https://www.who.int/teams/global-influenza-programme/avian-influenza/avian-a-h5n1-virus (accessed April 14, 2026).
8. R. Cao, B. Cao, Y. Hu, Z. Feng, D. Wang, W. Hu, J. Chen, Z. Jie, H. Qiu, K. Xu, X. Xu, H. Lu, W. Zhu, Z. Gao, N. Xiang, Y. Shen, Z. He, Y. Gu, Z. Zhang, Y. Yang, X. Zhao, L. Zhou, X. Li, S. Zou, Y. Zhang, X. Li, L. Yang, J. Guo, J. Dong, Q. Li, L. Dong, Y. Zhu, T. Bai, S. Wang, P. Hao, W. Yang, Y. Zhang, J. Han, H. Yu, D. Li, G. F. Gao, G. Wu, Y. Wang, Z. Yuan, Y. Shu, *N. Engl. J. Med.*, **368**, 1888-1897 (2013).
9. Z. Zhao, Z. Guo, C. Zhang, L. Liu, L. Chen, C. Zhang, Z. Wang, Y. Fu, J. Li, H. Shao, Q. Luo, J. Qian, L. Liu, *Sci. Rep.*, 2017, **7**, 16280.
10. S. Rafique, F. Rashid, S. Mushtaq, A. Ali, M. Li, S. Luo, L. Xie, Z. Xie, *Fornt. Microbiol.*, **2023**, 14, 1200681.
11. T. P. Peacock, J. James, J. E. Sealy, M. Iqbal, *Viruses*, 2019, **11**, 620.

Analyst Accepted Manuscript

View Article Online
DOI: 10.1039/D6AN00505E

Open Access Article. Published on 11 June 2026. Downloaded on 6/12/2026 3:26:18 AM.
This article is licensed under a Creative Commons Attribution 3.0 Unported Licence.

12. R. M. Cha, Y. Jang, M.-J. Park, J. Kim, J.-M. Kim, E. H. Lim, G.-B. Heo, S.-H. An, K.-N. Lee, Y.-J. Lee, E.-K. Lee, *Transbound. Emerg. Dis.*, **2026**, 2026, 8053623.
13. M.-W. Lin, I. A. Quintela, S. S. Sablani, C.-S. Lin, V. C. H. Wu, *J. Virol.*, 2025, **99**, e0148425.
14. S. Azeem, K.-J. Yoon, *Viruses*, 2025, **17**, 228.
15. European Commission. Breaking the spread of avian flu: new tools for faster detection. https://health.ec.europa.eu/one-health/zoonotic-threats/one-health-approach-zoonotic-avian-influenza_en (accessed April 14, 2026).
16. Q. Niu, Z. Jiang, L. Wang, X. Ji, G. Baele, Y. Qin, L. Lin, A. Lai, Y. Chen, M. Veit, S. Su, *Nat. Commun.*, 2025, **16**, 3558.
17. O. Wakao, K. Satou, A. Nakamura, K. Sumiyoshi, M. Shirokawa, C. Mizokuchi, K. Shiota, M. Maeki, A. Ishida, H. Tani, K. Shigemura, A. Hibara and M. Tokeshi, *Rev. Sci. Instrum.*, 2018, **89**, 024103.
18. O. Wakao, K. Satou, A. Nakamura, P. A. Galkina, K. Nishiyama, K. Sumiyoshi, F. Kurosawa, M. Maeki, A. Ishida, H. Tani, M. A. Proskurnin, K. Shigemura, A. Hibara and M. Tokeshi, *Lab Chip*, 2019, **19**, 2581-2588.
19. A. Nakamura, M. Aoyagi, M. Fukuyama, M. Maeki, A. Ishida, H. Tani, K. Shigemura, A. Hibara, M. Tokeshi, *ACS Food Sci. Technol.*, 2021, **1**, 1623-1628.
20. Y. Ogura, M. Fukuyama, M. Kasuya, K. Shigemura, S. A. Eremin, M. Tokeshi, *Anal. Sci.*, 2023, **39**, 2001-2006.
21. S. Chida, K. Takahashi, M. Fukuyama, M. Kasuya, A. Imai, A. V. Zherdev, S. A. Eremin, M. Maeki, A. Ishida, H. Tani, K. Shigemura, A. Hibara, M. Tokeshi, *Anal. Sci.*, in press.
22. M. Fukuyama, A. Nakamura, K. Nishiyama, A. Imai, M. Tokeshi, K. Shigemura, A. Hibara, *Anal. Chem.*, 2020, **92**, 14393-14397.
23. K. Nishiyama, Y. Takeda, M. Maeki, A. Ishida, H. Tani, K. Shigemura, A. Hibara, Y. Yonezawa, K. Imai, H. Ogawa, M. Tokeshi, *Sens. Actuators B*, 2020, **316**, 128160.
24. K. Nishiyama, K. Takahashi, M. Fukuyama, M. Kasuya, A. Imai, T. Usukura, N. Maishi, M. Maeki, A. Ishida, H. Tani, K. Hida, K. Shigemura, A. Hibara, M. Tokeshi, *Biosens. Bioelectron.*, 2021, **190**, 113414.
25. K. Takahashi, S. Chida, T. Suwatthanarak, M. Iida, M. Zhang, M. Fukuyama, M. Maeki, A. Ishida, H. Tani, T. Yasui, Y. Baba, A. Hibara, M. Okochi, M. Tokeshi, *Lab Chip*, 2022, **22**, 2971-2977.
26. K. Nishiyama, Y. Takeda, K. Takahashi, M. Fukuyama, M. Maeki, A. Ishida, H. Tani, K. Shigemura, A. Hibara, H. Ogawa, M. Tokeshi, *Anal. Bioanal. Chem.*, 2021, **413**, 4619-4623.

Analyst Accepted Manuscript

View Article Online
DOI: 10.1039/D6AN00505E

27. C. Yu-Ting, R. Suzuki, Y. Fujioka, A. Ishida, A. Imai, M. Fukuyama, M. Kasuya, Y. Ohba, T. Fukuhara, K. Shigemura, A. Hibara, M. Maeki, M. Tokeshi, *ACS Omega*, 2025, **10**, 51228-51235.
28. P. A. Routledge, A. D. Hutchings, in The Immunoassay Handbook, ed by D. Wild, 4th ed., Elsevier, Oxford, 2013, pp.945-962.
29. K. Nishiyama, M. Fukuyama, M. Maeki, A. Ishida, H. Tani, A. Hibara, M. Tokeshi, *Sens. Actuators B*, 2021, **326**, 128982.
30. W. B. Dandliker, V. A. de Saussure, *Immunochemistry,* 1970, **7,** 799–828.
31. F. Perrin, *J. Phys. Radium.*, 1926, **7**, 390-401.
32. ATTO 647N, Leica Microsystems, https://www.leica-microsystems.com/products/consumables/p/atto-647n/ (accessed April 17, 2026).
33. HiLyte™ Fluor 647, AnaSpec, https://www.anaspec.com/en/catalog/hilyte-fluor-647-succinimidyl-ester-se-1-mg~a3542919-7812-4c81-b170-2c86e5022084 (accessed April 17, 2026).
34. https://lifesciences.danaher.com/us/en/products/sku/ad-647n-31-leica.html (accessed April 17, 2026).
35. E. Spackman, *Methods Mol. Biol.*, 2008, **436**, 1-6.
36. O. D. Hendrickson, N. A. Taranova, A. V. Zherdev, B. B. Dzantiev, S. A. Eremin, *Sensors*, 2020, **20**, 7132.

Open Access Article. Published on 11 June 2026. Downloaded on 6/12/2026 3:26:18 AM.
This article is licensed under a Creative Commons Attribution 3.0 Unported Licence.

Analyst Accepted Manuscript

View Article Online
DOI: 10.1039/D6AN00505E

Open Access Article. Published on 11 June 2026. Downloaded on 6/12/2026 3:26:18 AM.
This article is licensed under a Creative Commons Attribution 3.0 Unported Licence.

Figure captions

Figure 1 Fluorescence polarization analyzer (a) and microfluidic device (b) for NC-FPIA. The analyzer has dimensions of W 35 cm × D 15 cm × H 15 cm and weighs 5.5 kg. The disposable 9-microchannel microfluidic device, capable of simultaneously analyzing nine samples, was fabricated by bonding a black PDMS substrate fabricated using soft lithography to a glass plate. The microchannels had a width of 200 μm and a depth of 900 μm. Samples were introduced into each microchannel (12 μL per microchannel) using a pipette through a 3D-printed interface.

Figure 2 Schematic illustration of NC-FPIA for H5-AIV detection using fluorophore-labeled Fab. Free fluorophore-labeled Fab undergoes rapid rotational motion in solution, and even when excited with polarized light, the emitted fluorescence becomes depolarized, resulting in a low fluorescence polarization. In contrast, when the fluorophore-labeled Fab binds to the HA of H5-AIV, the rotational motion of the resulting complex becomes slower, and the emitted fluorescence remains polarized, resulting in a high fluorescence polarization.

Figure 3 Dependence of polarization change (ΔP) on tracer concentration. H5N3 AIV concentration was 850 μg/mL. Bars represent mean values, with error bars indicating standard deviation (n = 3). $\Delta mP = 10^3 \times \Delta P$ ($= P_{sample} - P_{control}$).

Figure 4 Calibration curves for purified H5N3 AIV obtained at an ATTO-Fab concentration of 120 ng/mL. For the measurements, purified H5N3 AIV, PBS, 120 ng/mL ATTO-Fab solution, and 1% BSA solution were mixed in a volume ratio of 7:1:1:1. Data points represent mean values (n = 3), with error bars

Analyst Accepted Manuscript

View Article Online
DOI: 10.1039/D6AN00505E

indicating standard deviation. The solid line represents the fitted curve based on the four-parameter logistic (4PL) model. $\Delta mP = 10^3 \times \Delta P$ ($= P_{sample} - P_{control}$).

Figure 5 Fluorescence intensity as a function of the dilution factor of avian oropharyngeal swab samples. Bars represent mean values (n = 3), with error bars indicating standard deviation. The dashed line indicates the fluorescence intensity of ATTO-Fab (120 ng/mL).

Figure 6 Calibration curve for H5N3 AIV in avian oropharyngeal swab samples at an ATTO-Fab concentration of 120 ng/mL. For the measurements, purified H5N3 AIV, diluted swab samples, 120 ng/mL ATTO-Fab solution, and 1% BSA solution were mixed in a volume ratio of 7:1:1:1. Data points represent mean values (n = 3), with error bars indicating standard deviation. The solid line represents the fitted curve based on the four-parameter logistic (4PL) model. $\Delta mP = 10^3 \times \Delta P$ ($= P_{sample} - P_{control}$).

Open Access Article. Published on 11 June 2026. Downloaded on 6/12/2026 3:26:18 AM.
This article is licensed under a Creative Commons Attribution 3.0 Unported Licence.

Analyst Accepted Manuscript

View Article Online
DOI: 10.1039/D6AN00505E

Date availability

All the experimental data are presented in the main text and supplementary information (SI). Supplementary information is available. See DOI: https://doi.org/10.1039/XXXX. Other information is available upon reasonable request from the corresponding author.

Open Access Article. Published on 11 June 2026. Downloaded on 6/12/2026 3:26:18 AM.
This article is licensed under a Creative Commons Attribution 3.0 Unported Licence.

Analyst Accepted Manuscript

Open Access Article. Published on 11 June 2026. Downloaded on 6/11/2026 4:42:14 PM.
This article is licensed under a Creative Commons Attribution 3.0 Unported Licence.

Figure 1

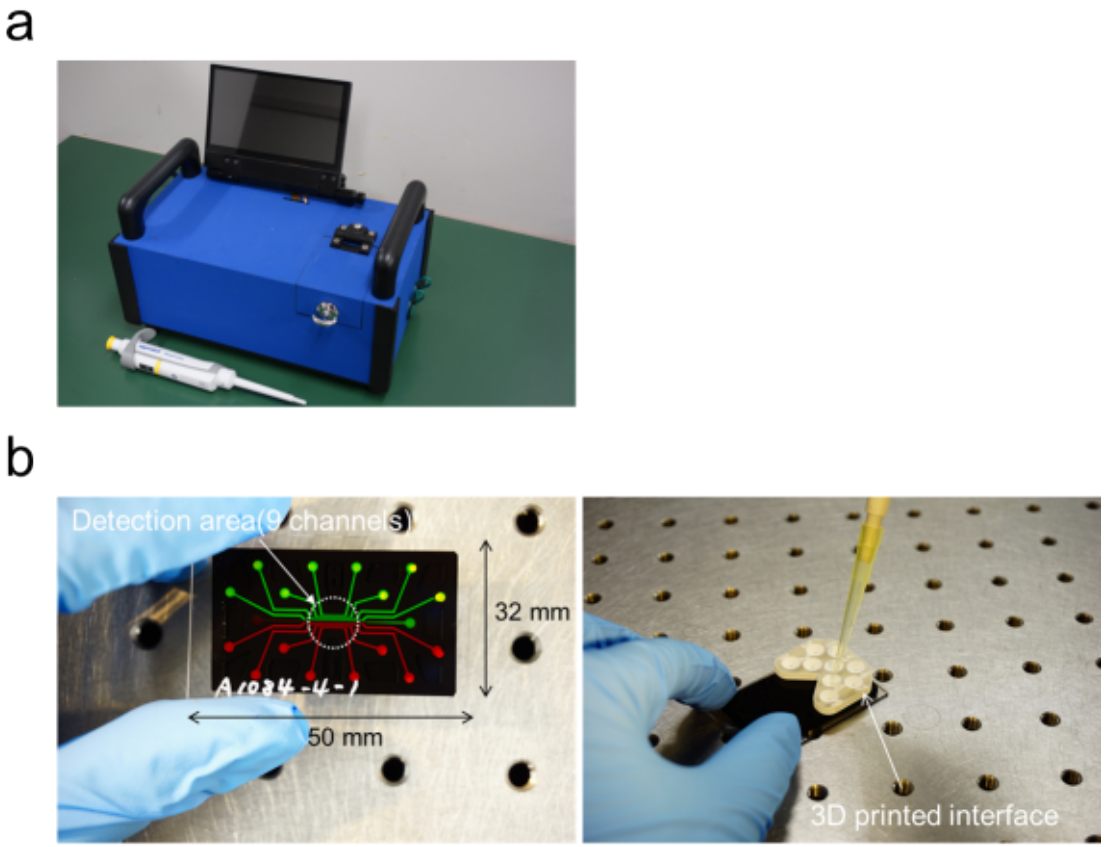

Analyst Accepted Manuscript

Open Access Article. Published on 11 June 2026. Downloaded on 6/1
This article is licensed under a Creative Commons Attrib

Figure 2

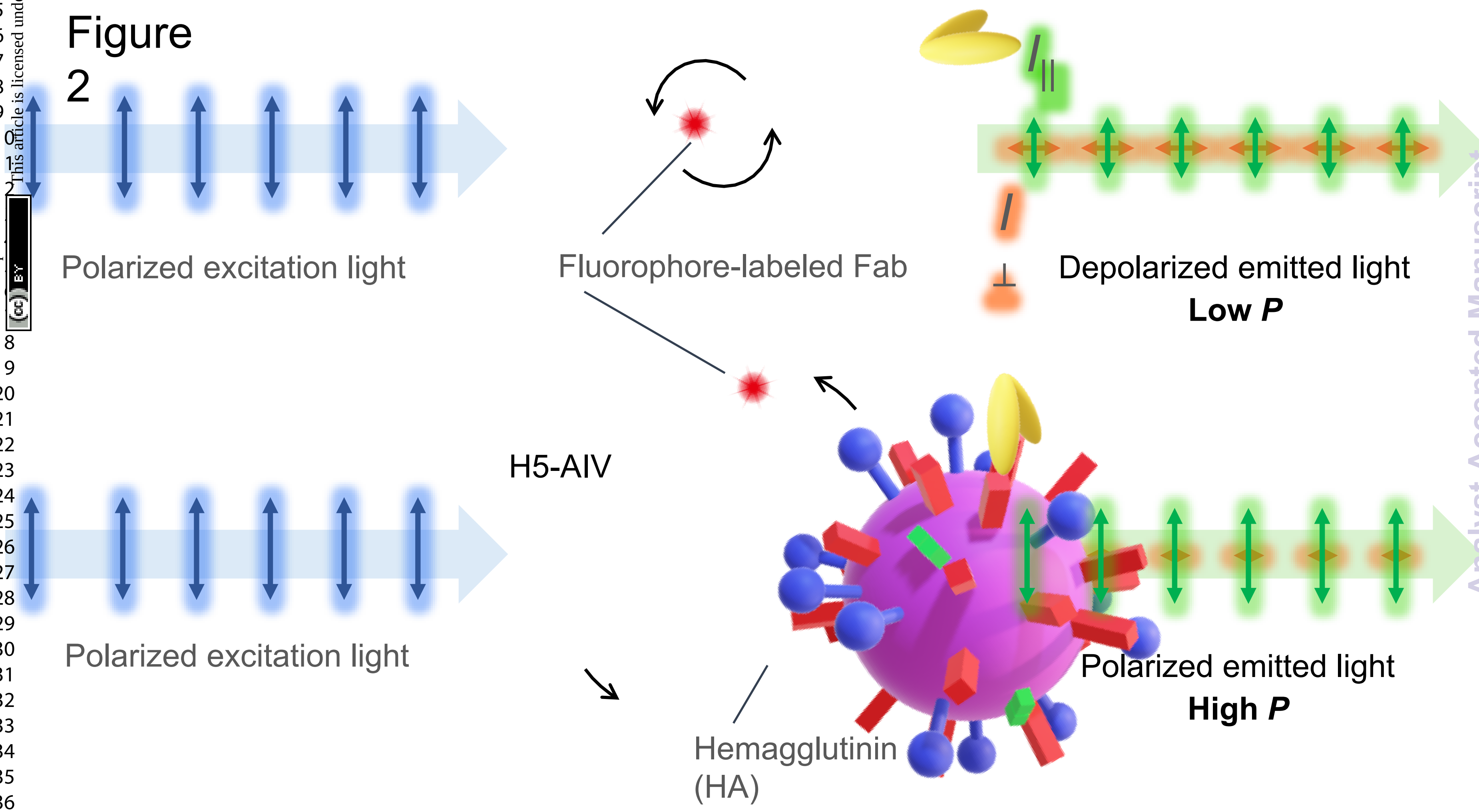

Analyst Accepted Manuscript

Open Access Article. Published on 11 June 2026. Downloaded on 6/1
This article is licensed under a Creative Commons Attrib

Figure 3

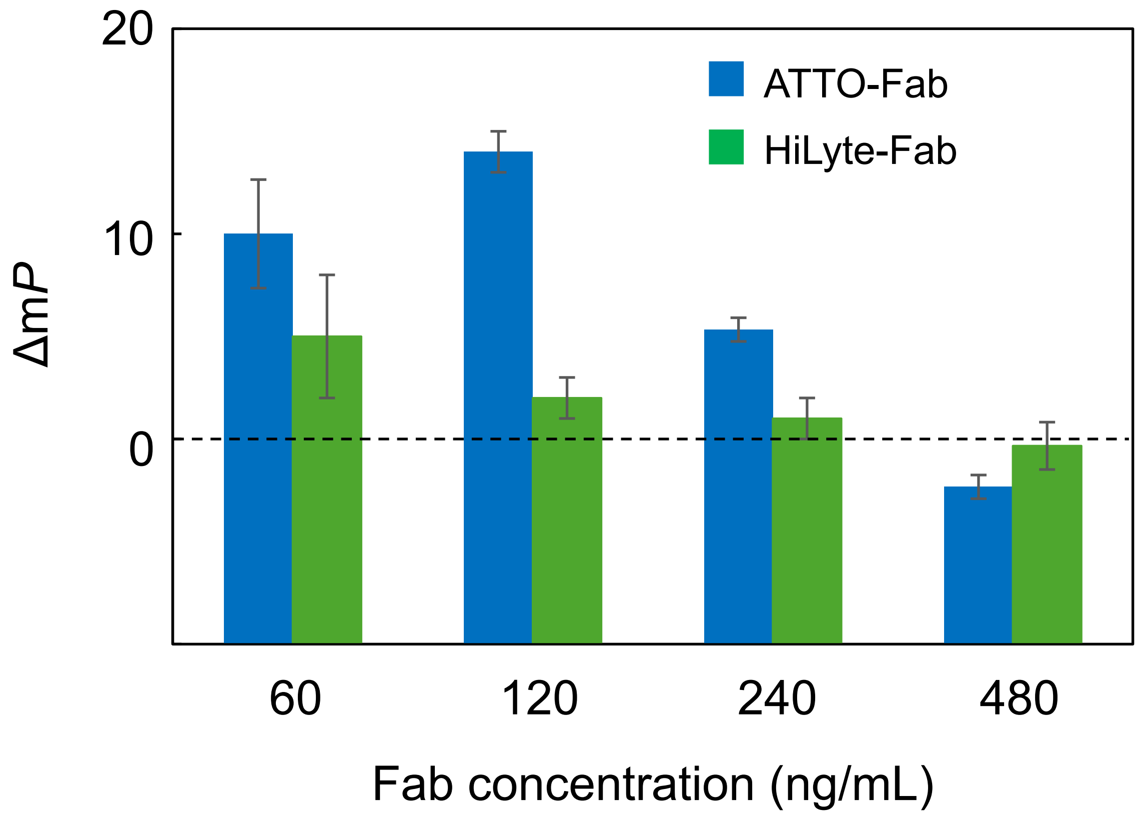

Analyst Accepted Manuscript

Open Access Article. Published on 11 June 2026. Downloaded on 6/1
This article is licensed under a Creative Commons Attribution

Figure 4

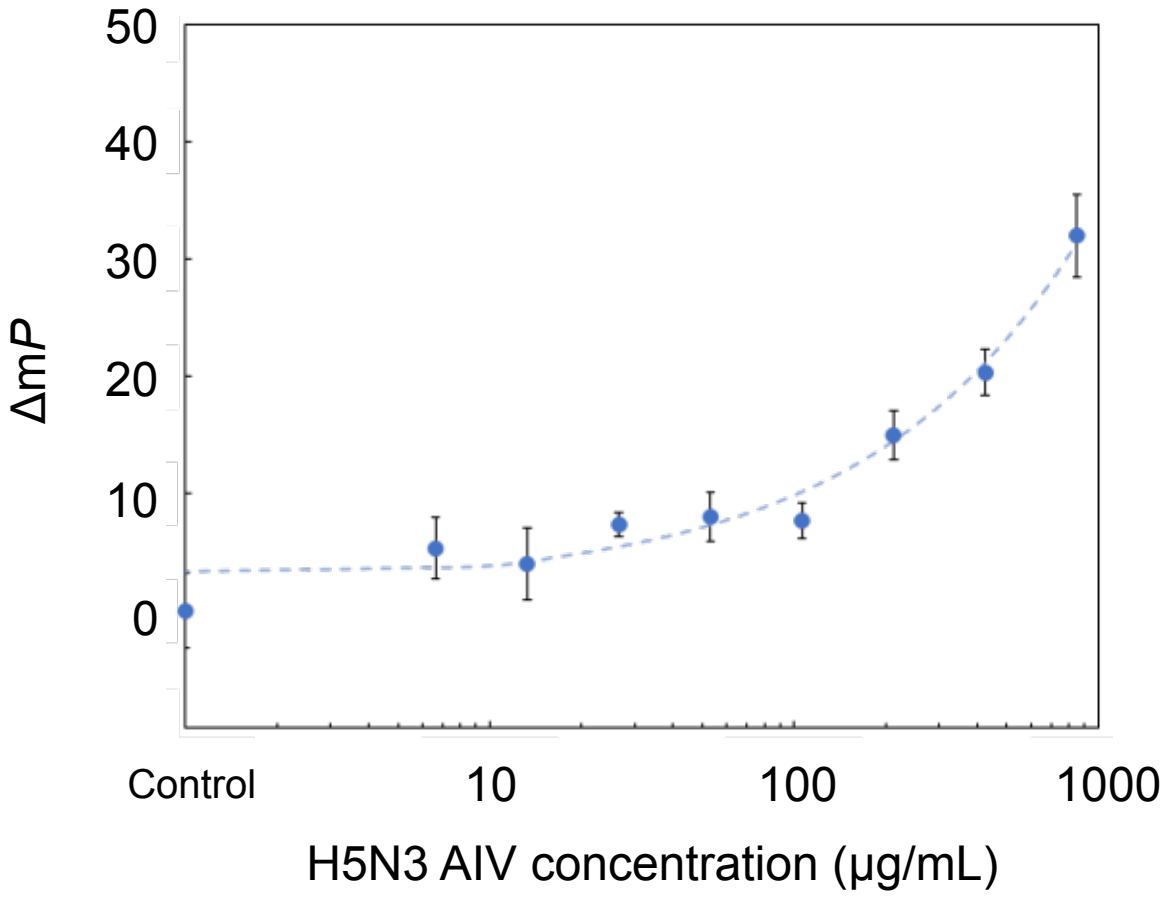

Analyst Accepted Manuscript

Open Access Article. Published on 11 June 2026. Downloaded on 6/11/2026 4:42:32 AM.
This article is licensed under a Creative Commons Attribution 3.0 Unported Licence.

Figure 5

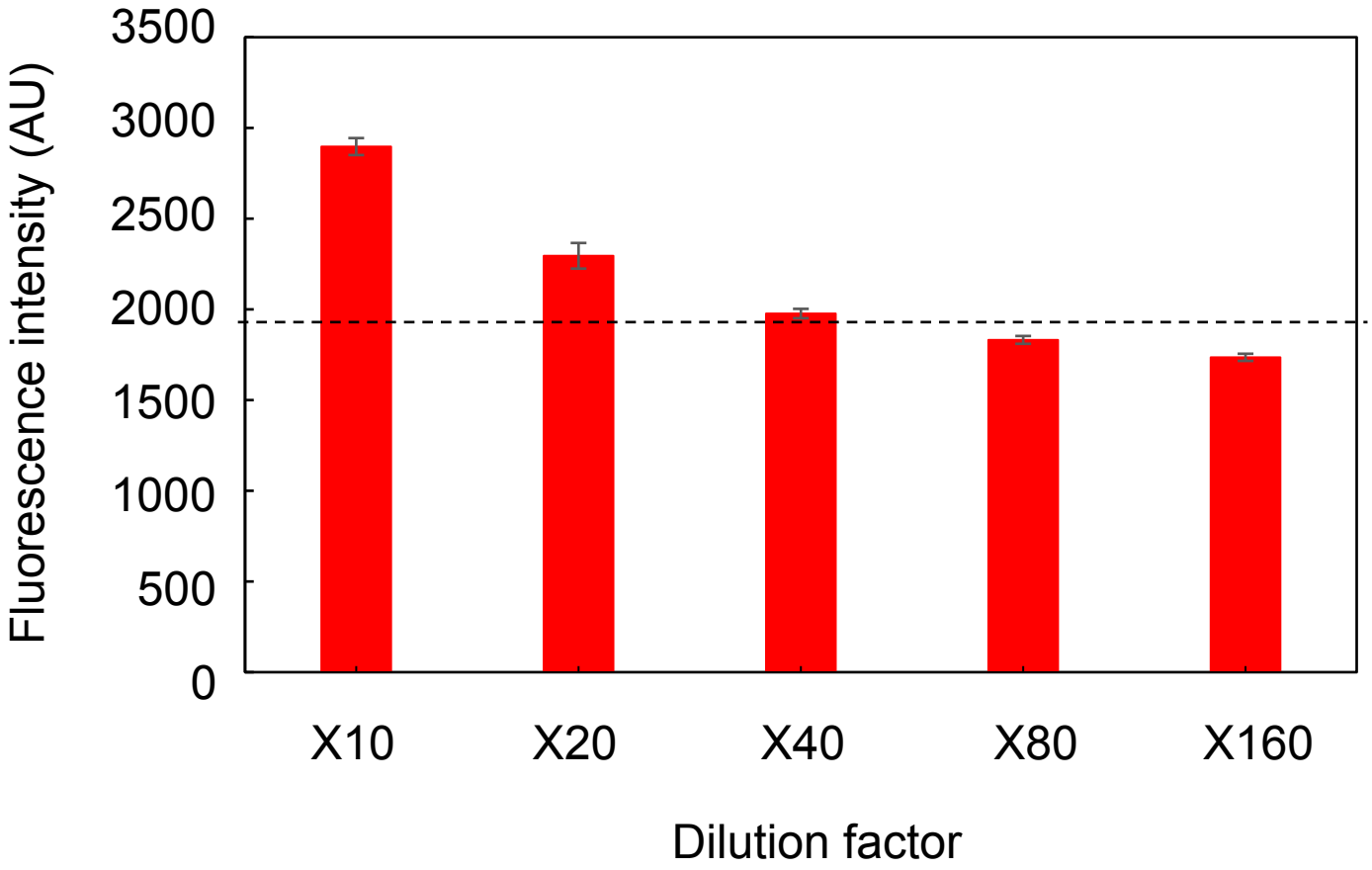

Analyst Accepted Manuscript

Open Access Article. Published on 11 June 2026. Downloaded on 6/1
This article is licensed under a Creative Commons Attrib

Figure 6

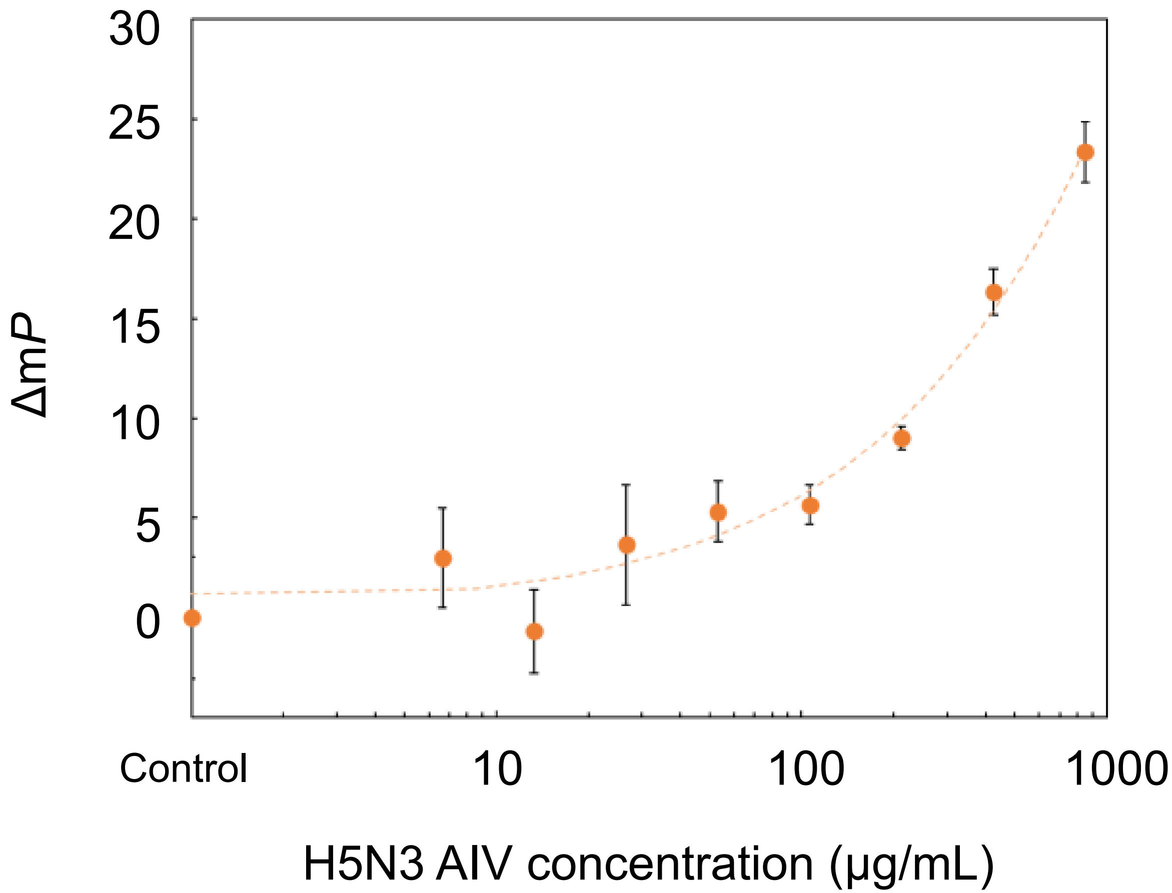

Analyst Accepted Manuscript

View Article Online
DOI: 10.1039/D6AN00505E

Date availability

All the experimental data are presented in the main text and supplementary information (SI). Supplementary information is available. See DOI: https://doi.org/10.1039/XXXX. Other information is available upon reasonable request from the corresponding author.

Open Access Article. Published on 11 June 2026. Downloaded on 6/12/2026 3:26:18 AM.
This article is licensed under a Creative Commons Attribution 3.0 Unported Licence.

Analyst Accepted Manuscript